SCIENTIFIC REPORTS

OPEN

Correspondence and
requests for materials
should be addressed to
L.I.J. (lejoh@ifm.liu.se)

Multiple π-bands and Bernal stacking of multilayer graphene on C-face SiC, revealed by nano-Angle Resolved Photoemission

Leif I. Johansson[1], Rickard Armiento[1], Jose Avila[2], Chao Xia[1], Stephan Lorcy[2], Igor A. Abrikosov[1], Maria C. Asensio[2] & Chariya Virojanadara[1]

[1]Department of Physics, Chemistry and Biology, Linköping University, SE-58183 Linköping, Sweden, [2]Synchrotron SOLEIL, L'Orme des Merisiers, Saint Aubin-BP 48, 9192 Gif sur Yvette Cedex, France.

Only a single linearly dispersing π-band cone, characteristic of monolayer graphene, has so far been observed in Angle Resolved Photoemission (ARPES) experiments on multilayer graphene grown on C-face SiC. A rotational disorder that effectively decouples adjacent layers has been suggested to explain this. However, the coexistence of μm-sized grains of single and multilayer graphene with different azimuthal orientations and no rotational disorder within the grains was recently revealed for C-face graphene, but conventional ARPES still resolved only a single π-band. Here we report detailed nano-ARPES band mappings of individual graphene grains that unambiguously show that multilayer C-face graphene exhibits multiple π-bands. The band dispersions obtained close to the $\bar{K}$-point moreover clearly indicate, when compared to theoretical band dispersion calculated in the framework of the density functional method, Bernal (AB) stacking within the grains. Thus, contrary to earlier claims, our findings imply a similar interaction between graphene layers on C-face and Si-face SiC.

Graphene-based two-dimensional science has made a major impact on both fundamental and applied condensed matter physics[1,2]. Epitaxial graphene grown on the basal planes of silicon carbide is considered a most promising route[3] for the development of carbon based nano-electronics. Large-scale epitaxial films with atomic layer defined termination, highly desirable for applications as well as for fundamental and functionalization studies, have been grown[4,5] on Si-terminated SiC substrates. On the C-terminated SiC(000-1) surface graphene films with similarly large scale uniformity has so far[6–9] not been possible to produce.

Epitaxial graphene prepared on C-face SiC has moreover been claimed[10–13] to be fundamentally different compared to Si-face graphene. Whereas Si-face graphene exhibits sharp Low Energy Electron Diffraction (LEED) spots and Bernal (AB) stacking, the macro LEED diffraction pattern published from C-face graphene was smeared out into a strongly modulated diffraction ring[6,11–13]. This, together with Surface X-ray diffraction results[10,11,13] and moiré patterns observed[14] in STM topographs, was interpreted to indicate that the graphene layers on the C-face stack in such a way that adjacent layers are rotated with respect to each other. This rotational disorder was suggested to explain[11,13,15–17] why epitaxial graphene films, about ten layers thick, in conventional ARPES measurements show single layer electronic properties, i.e. a single linearly dispersing π-band with the Dirac point located close to the Fermi level. Graphene on the C-face has therefore been called multilayer epitaxial graphene[18] and suggested to order azimuthally in a particular way with alternating rotations of the layers, which results in an electronic band structure of isolated/decoupled graphene layers. This is very different compared to the band structure of Si-face Bernal stacked graphene[19] where only a single graphene layer gives rise to one π-band cone and linearly dispersing bands close to the $\bar{K}$-point. Bi- and tri-layer graphene[2,19,20] give rise to two and three cones, respectively, and π-bands showing a non-linear dispersion close to the $\bar{K}$-point.

Because of these reported fundamental differences between C-face and Si-face graphene we have studied graphene samples sublimation grown on nominally on-axis C-face SiC. Low Energy Electron Microscopy (LEEM), X-ray Photo Electron Electron Microscopy (XPEEM), and selected area LEED (micro-LEED) data shows[8,9] formation of fairly large (some μm) grains (crystallographic domains) of graphene exhibiting sharp (1 × 1) spots in micro-LEED, and different azimuthal orientations of adjacent grains. The C-face graphene
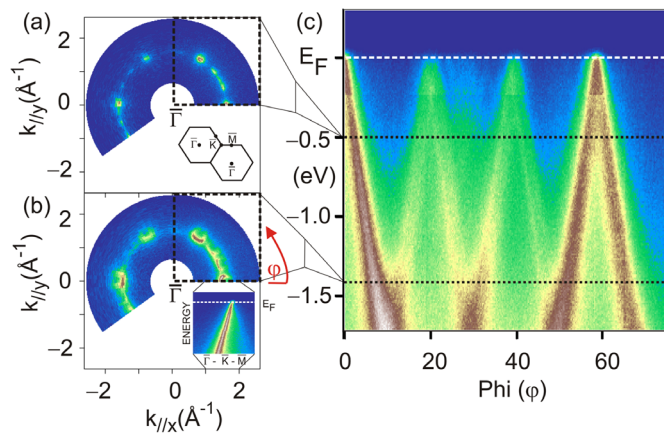
Figure 1 | Constant initial energy photoelectron angular distribution pattern, $E_i(k_x,k_y)$, extracted at (a) 0.5 eV and (b) 1.4 eV below the Fermi energy, from two sets of micro-ARPES data recorded at 100 eV photon energy. One set was collected at azimuthal angles from 0° to 225° in 3° steps (of which the range 90° to 220° is displayed) and the second set from 0° to 90° in steps of 0.25° (displayed in the figure). (c) A cut at $k_{//} =$ sqrt($k_x^2+k_y^2$) = 1.72 Å^{-1} from the second set of micro-ARPES data collected from 0° to 90° in steps of 0.25°, representing a circular cut through the two dominant $\bar{K}$-points, observed in this azimuthal angle range in (a) and (b). The inset in (a) shows two Brillouin zones and the directions referred to. The micro-ARPES spectrum of the π-band structure, shown as inset in (b), was collected at an electron emission angle (θ_e) that correspond to probing around the $\bar{K}$-point and along one $\bar{\Gamma}-\bar{K}-\bar{M}$ direction (azimuthal angle φ = 0°).

sample utilized in the present ARPES study has these characteristics and grains with a thickness ranging from one to seven layers (see Fig. S1 in Supplementary information). However, only one π-band cone could be resolved at the $\bar{K}$-point using conventional ARPES[8,13,21] or XPEEM[8,9], i.e. in selected area constant initial energy photoelectron angular distribution patterns, although LEEM showed multilayer graphene on most parts of the sample surface. If the graphene layers are not rotationally disordered more than one π-band should definitely be observed[2,19,20] from a multilayer graphene grain having any of the common stacking sequences, Rhombohedral (ABC), Bernal (AB) or simple hexagonal (AA) stacking (see Fig. S2 in Supplementary information). However, conventional ARPES does not have the lateral resolution[8,12,21] to investigate single grains on C-face graphene samples and in the XPEEM measurements[8,9] high enough energy and momentum resolutions could not be achieved to resolve if multilayer grains exhibited more than one π-band.

The micro- and nano-ARPES end station at the ANTARES beamline[22,23] offers a lateral resolution of ca. 90 μm and 120 nm, respectively. At the same time it allows an overall energy and momentum resolution of 5 meV and 0.005 Å^{-1} at 100 eV photon energy in nano-ARPES measurements. Thus, nano-ARPES opens up the possibility to perform detailed studies of the electron band structure from the μm-sized graphene grains typically forming on C-face samples. Micro-, or multigrain-ARPES analysis, on the other hand, can be used to investigate the distribution of azimuthal angles of the grains and determine the dominant azimuthal orientation present. Information about this is also directly visible in macro-LEED patterns, as shown below.

A micro-ARPES spectrum of the π-band structure collected at an electron emission angle (θ_e) that corresponds to probing around the $\bar{K}$-point and along one $\bar{\Gamma}-\bar{K}-\bar{M}$ direction (azimuthal angle φ = 0°), is shown in the inset of Fig. 1. From sets of such spectra recorded at azimuthal angles from 0° to 220° the constant initial energy photoelectron angular distribution patterns, $E_i(k_x,k_y)$, displayed in the two semicircular segments in Figs. 1(a) and (b) are extracted, at energies
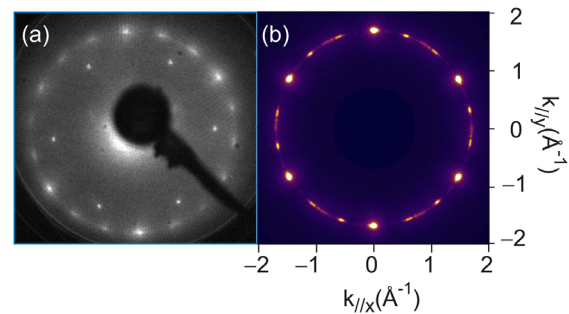

Figure 2 | (a) A macro-LEED pattern collected at 79 eV, showing that the dominant orientation of the graphene grains is rotated 30° relative to the SiC substrate while the two sets of weaker and more elongated diffraction spots are rotated about ±10° relative to the SiC substrate. The inner six spots represent the (1 × 1) diffraction pattern of the SiC substrate. (b) Fermi surface (E_i = 0 eV) constructed from the second set of micro-ARPES data, collected at azimuthal angles from 0° to 90°, and displayed rotated in such a way that the directions of the dominant and minor features in (a) and (b) coincide.

of respectively 0.5 eV and 1.4 eV below the Fermi energy. Three additional $\bar{K}$-points at azimuthal angles of around 60°, 120° and 180° are clearly observed in these segments, but also additional features that originate from graphene grains of different orientations. This is even more clearly illustrated in Fig. 1(c), which shows a circular cut through the two first main $\bar{K}$-points in Figs. 1(a) and (b). At φ ≈ 0° half a Dirac cone and at φ ≈ 60° a full Dirac cone are clearly observed. These main Dirac cones show linear dispersion close to the $\bar{K}$-point, similar to earlier reported conventional ARPES results[8,13,21]. The bands are quite broad, however, so they may contain contributions from several unresolved bands. Two weaker Dirac cones are also visible at φ around 20° and 40°. These latter cones originate from graphene grains with different azimuthal orientations and correspond to the additional features observed in between the dominant $\bar{K}$-points in Figs. 1(a) and (b). The macro-LEED pattern recorded from the sample, see Fig. 2(a), also reveals one dominant and two additional fairly equally favored orientations of the graphene grains. The Fermi surface constructed from the micro-ARPES data is displayed in Fig. 2(b), for comparison. In both pictures the weaker additional diffraction spots/$\bar{K}$-points appear elongated which we interpret to indicate a larger spread in the azimuthal orientation of these grains compared to those contributing to the dominant spots/$\bar{K}$-points.

For the purpose to distinguish the graphene grains on the sample, using nano-ARPES, the scanning mode of the ANTARES microscope was utilized. The result when setting the analyzer to measure the integrated intensity of photoelectrons, at the $\bar{K}$-point at φ = 59° and in 0.5 μm steps over the sample, is shown in Fig. 3(a). Only grains having this dominant azimuthal orientation should give any appreciable intensity and multilayer grains higher intensity than monolayer graphene grains. The four locations labeled B, C, D and E in Fig. 3(a), were among the positions selected to collect nano-ARPES spectra from. The resulting spectra, displayed in separate panels, show (b) one, (c) three, (d) four and (e) five π-bands. The color labeling increases from blue-green to orange-red at the four locations labeled B to E. A straightforward conclusion is that the number of π-bands reflects the number of graphene layers in different grains. From the purple/darkest blue areas no π-band contribution is discernable so these areas correspond to locations where the graphene grains have a different azimuthal orientation. The same procedure to map the intensity and select positions to collect nano-ARPES spectra from, was repeated at φ = 39°, which correspond to one of the weaker cones in Fig. 1(c). Two spectra are displayed in (f) and (g) and show one and two π-bands, respectively. The azimuthal
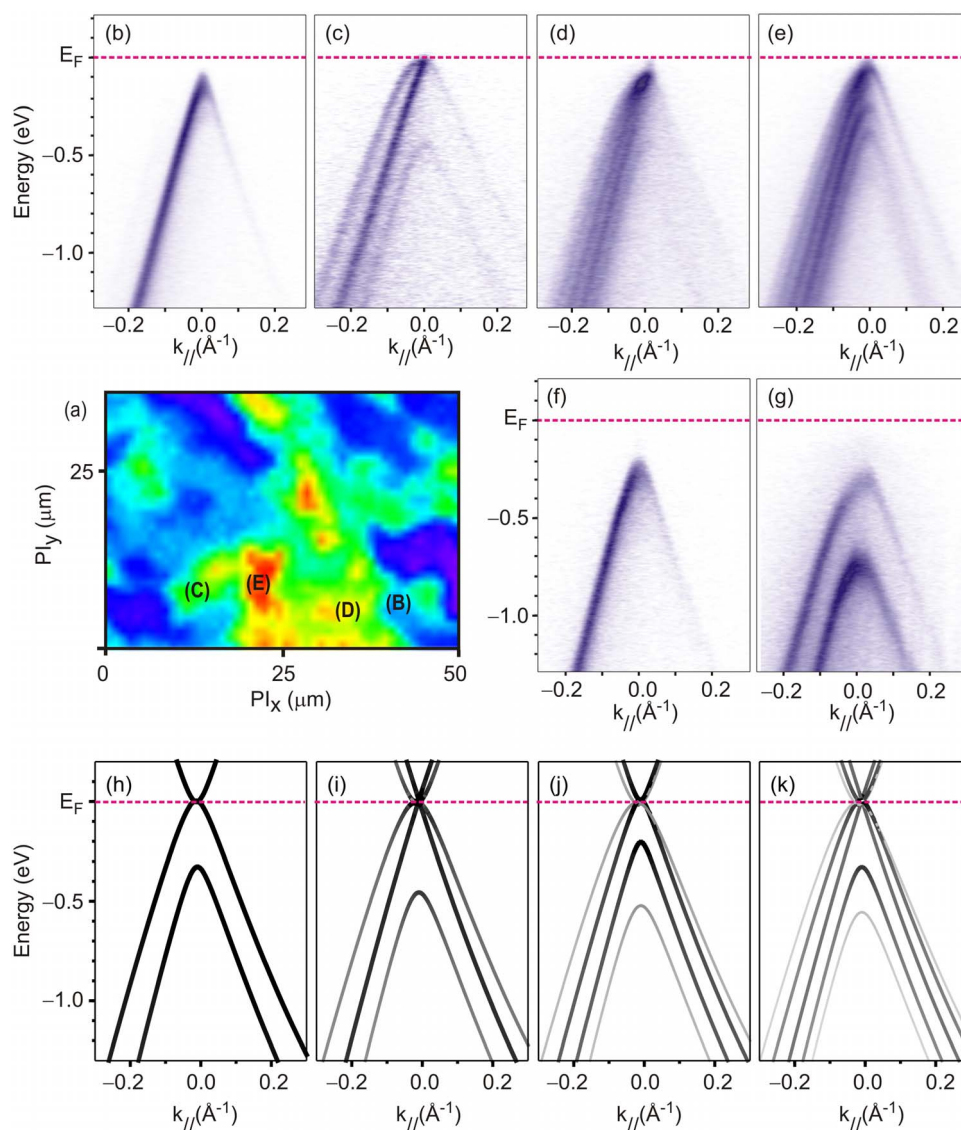
Figure 3 | (a) A two-dimensional nano-ARPES image of the measured integrated intensity of the graphene π-band(s) in the energy range 0 to 0.5 eV below the Fermi level and at the $\bar{K}$-point at φ = 59° (see Fig. 1). The area shown is 35 × 50 μm², the photon energy used 100 eV, and the intensity is provided in a linear scale as a color image. (b)-(e) Nano-ARPES spectra recorded, at φ = 59° along the $\bar{\Gamma} - \bar{K} - \bar{M}$ direction and at hν = 100 eV, from four different graphene grains at the correspondingly labeled positions in (a). In (f) and (g) similar nano-ARPES spectra recorded at φ = 39° from two different graphene grains at other positions on the surface are shown. Theoretical π-band dispersions calculated for (h) two, (i) three, (j) four and (k) five layers of Bernal stacked free standing graphene, using density functional theory.

angle is obviously almost 1° off from the correct $\bar{\Gamma} - \bar{K} - \bar{M}$ direction for these grains, since the π-cones are not cut through their centers so an "apparent[23] band gap" appears. It deserves to be mentioned that the grains probed in this azimuth shows only one or two π-bands and clearly a larger spread in the azimuthal orientation of the grains. If one looks carefully in Figs. 3(b)–(e) one can also notice a variation in the location of the π-band maximum relative to the Fermi level, although smaller, implying a small variation in the orientation[24] also of the grains contributing to the dominant cones. This should, how-ever, not affect the band structure within a grain and the goal to determine if more than one π-band could be resolved from grains of multilayer graphene on C-face SiC. The nano-ARPES spectra displayed in Fig. 3 illustrate clearly that grains are identified and that one can resolve from one and up to five π-bands. This corresponds well to the LEEM data from this sample, which shows grains with a thickness ranging from one to seven layers of graphene (see Fig. S1 in Supplementary information). The nano-ARPES spectra thus dem-onstrate unambiguously that also C-face graphene exhibits multiple

π-bands from grains having multiple layers of graphene. The Dirac point is in Figs. 3(b)–(e) seen to be located fairly close to the Fermi level in grains having from one to five layers of graphene. This is noticeably different compared to Si-face graphene[19] where the Fermi level is displaced 0.45 eV above the Dirac point for monolayer gra-phene, due to electron transfer from the substrate.

The stacking within the graphene grains can be determined from the differences in π-band dispersions close to the $\bar{K}$-point for free standing graphene for different stacking sequences[2,20] (see Figs. S2 and S3 in supplementary information). We find a striking similarity between the experimental results and the theoretical band structure for Bernal stacked graphene shown in Figs. 3(h)–(k), calculated in the framework of the density functional theory[25,26] (see method section for computational details). Other stacking sequences considered, e.g., rhombohedral and simple hexagonal, can be ruled out as they give qualitatively different band dispersions (see Figs. S2 and S3 in Supplementary information). In the theoretical band structure, the separation between the outermost bands at the $\bar{K}$-point increases

from 0.33 eV for two layers to 0.56 eV for five layers, which compares well with the separation seen in Figs. 3(b)–(g). The line thickness and shade of the calculated band segments in Figs. 3(h)–(k) show the overlap onto s and p states on the atoms at the topmost layer of graphene. Hence, darker bands have higher relative surface character and they are expected to be more clearly distinguishable in surface sensitive experiments, which is in close agreement with the experimental results. Therefore, our theoretical results also clarify the variation in the intensity of the band dispersions. The comparison between theoretical and experimental band dispersions thus clearly shows that the layers within the multilayer graphene grains on C-face SiC are Bernal stacked, like in the case of graphene[19] on Si-face SiC, which also implies that the interaction between graphene layers is similar.

In conclusion, utilizing nano-ARPES we have unambiguously revealed that multilayer graphene grains formed on C-face carbon show multiple π-bands and that only monolayer graphene grains exhibit a single π-band with linear dispersion. Moreover, the experimental dispersions for two to five layers of graphene are shown to closely resemble the theoretical band dispersions for Bernal stacked free standing graphene layers. Thus, contrary to earlier claims, the band structure and stacking of graphene on C-face SiC is shown to be similar to graphene grown on Si-face SiC, which implies that the interaction between graphene layers is also similar for the two surfaces.

Methods

Sample preparation. Graphene was grown[8,9] on the C-face of nominally on-axis, production grade n-type, 6H-SiC substrates from SiCrystal, having a mis-orientation error within 0.06°. High temperature sublimation in a graphite cell and in an argon buffer ambient with the following conditions was used: temperature 1900°C, pressure 850 mbar and a growth time of 15 min. The samples prepared in this way were transferred through the air to respectively the LEEM and ARPES end stations. There they were cleaned in ultrahigh vacuum by annealing at ca. 500°C for a few minutes and core level and valence band data recorded showed no trace of contaminants. Data collected at the Spectroscopic Photoemission and Low Energy Electron Microscope (SPELEEM) (Elmitec Gmbh) end station, at the MAX laboratory, showed the sample to have a very similar surface morphology, i.e. size and distribution of grains with different number of graphene layers and azimuthal orientations, as earlier reported[8,9] C-face samples.

ARPES experiments. Micro- and nano-ARPES experiments were performed at the ANTARES beamline[22,23] of the SOLEIL laboratory, France. Most of the ARPES data have been taken at a photon energy of 100 eV, using linearly polarized light, a base pressure of 5×10^{-11} torr and keeping the sample cooled at ca. 40 K.

The ANTARES beamline[22,23] is equipped with a Scienta R4000 hemisperical electron analyzer with a detection system based on a 40 mm diameter multi-channel plate detector. The wide angle lens of the detector, set with an acceptance angle of 25° or 14°, has excellent angular and transmission properties for accurate and fast band mappings. The nano-ARPES microscope of ANTARES is equipped with two Fresnel zone plates (FZP) responsible for the focalization of the synchrotron radiation and an order selection aperture to eliminate higher diffraction orders. The sample is mounted on a nano-positioning stage placed at the coincident focus of the Scienta analyzer and the FZP focal point. The spatial resolution is determined by the FZP resolution and the mechanical stability of sample stage. This innovative instrument is therefore excellently suited to determine the band structure of nano-sized samples. The microscope has two operating modes[22,23], the point mode, where ARPES spectra are collected from a nano- or micro-size area of the sample and a scanning mode, where the intensity of selected electron states of given momentum and energy is mapped over the sample so a two dimensional image of that particular electronic feature is generated.

Electronic band structure calculations. The band structure was calculated using *ab-initio* Kohn-Sham density functional theory[25,26] (DFT), as implemented in VASP[27,28] 5.2.11 using the projector augmented wave (PAW) scheme[29] and the exchange-correlation functional of Perdew, Burke and Erzernhof[30] (PBE). The plane-wave energy cutoff was set to 600 eV. A Monkhorst-Pack $12 \times 12 \times 1$ k-point mesh was used. The unit cells are slabs of N layers of freestanding graphene with various stackings (i.e., the substrate was not included). The structural parameters for the graphene layers are based on accepted values for graphite, i.e., perfect hexagonal layers with lattice constant 2.461 Å and an interlayer distance of 3.354 Å. We do not perform any structural relaxations since such relaxation in the presence of van der Waals forces is nontrivial in semi-local DFT. A vacuum separation of 15 Å was used for the periodic boundary conditions between slabs. To decorate bands in band structure plots according to projections onto atomic-like states has become known as the 'fat bands' method. For this purpose, VASP calculates the projections of the orbitals onto spherical harmonics within spheres around each atom with a radius

somewhat reduced from the value of the Wigner-Seitz radius (for C the radius used is 1.640 Å). For the band structure plot we calculated energy eigenstates at a 256 k-points on the high symmetry line through the Gamma point. Each separate segment between two such points is drawn with a line thickness and shade based on the total summed projection onto all angular momentum states for the C atoms on the topmost surface layer. The shading was normalized to full black for the largest summed projection. The intensity and width of the bands thus indicate their relative surface character.

1. Geim, A. K. & Novoselov, K. S. The rise of graphene. *Nature Mater.* **6**, 183–191 (2007).
2. Neto, A. H. C., Guinea, F., Peres, N. M. R., Novoselov, K. S. & Geim, A. K. The electronic properties of graphene. *Rev. Mod. Phys.* **81**, 109 (2009).
3. Berger, C. *et al.* Electronic Confinement and Coherence in Patterned Epitaxial Graphene. *Science* **312**, 1191–1196 (2006).
4. Virojanadara, C. *et al.* Homogeneous large-area graphene layer growth on 6H-SiC(0001). *Phys. Rev. B* **78**, 245403 (2008).
5. Emtsev, K. V. *et al.* Towards wafer-size graphene layers by atmospheric pressure graphitization of silicon carbide. *Nature Mater.* **8**, 203 (2009).
6. Luxmi, Srivastava, N., He, G., Feenstra, R. M. & Fisher, P. J. Comparison of graphene formation on C-face and Si-face SiC{0001} surfaces. *Phys. Rev. B* **82**, 235406 (2010).
7. Mathieu, C. *et al.* Microscopic correlation between chemical and electronic states in epitaxial graphene on SiC(000-1). *Phys. Rev. B* **83**, 235436 (2011).
8. Johansson, L. I. *et al.* The stacking of adjacent graphene layers grown on C-face SiC. *Phys. Rev. B.* **84**, 125405 (2011).
9. Johansson, L. I. *et al.* Is the registry between adjacent graphene layers grown on C-face SiC different compared to that on Si-face SiC. *Crystals* **3**, 1 (2013).
10. Hass, J. *et al.* Structural properties of the multilayer graphene/4H-SiC(000-1) system as determined by surface x-ray diffraction. *Phys. Rev. B* **75**, 214109 (2007).
11. Hass, J. *et al.* Why multilayer graphene on 4H-SiC(000-1) behaves like a single sheet of graphene. *Phys. Rev. Lett.* **100**, 125504 (2008).
12. Emtsev, K. V., Speck, F., Seyller, Th., Ley, L. & Riley, J. D. Interaction, growth, and ordering of epitaxial graphene on SiC{0001} surfaces: A comparative photoelectron spectroscopy study. *Phys. Rev. B* **77**, 155303 (2008).
13. Sprinkle, M. *et al.* First direct observation of a nearly ideal graphene band structure. *Phys. Rev. Lett.* **103**, 226803 (2009).
14. Miller, D. L. *et al.* Structural analysis of multilayer graphene via atomic moire interferometry. *Phys. Rev. B* **81**, 125427 (2010).
15. Lopes dos Santos, J. M. B., Peres, N. M. R. & Castro Neto, A. H. Graphene Bilayer with a Twist: Electronic Structure. *Phys. Rev. Lett.* **99**, 256802 (2007).
16. Latil, S., Meunier, V. & Henrard, L. Massless fermions in multilayer graphitic systems with misoriented layers: *Ab initio* calculations and experimental fingerprints. *Phys. Rev. B* **76**, 201402 (2007).
17. Mele, E. J. Commensuration and interlayer coherence in twisted bilayer graphene. *Phys. Rev. B* **81**, 161405 (2010); Band symmetries and singularities in twisted multilayer graphene. *Phys. Rev. B* **84**, 235439 (2011).
18. Ruan, M. *et al.* Epitaxial graphene on silicon carbide: Introduction to structured graphene. *MRS Bull.* **37**(12), 1138 (2012).
19. Ohta, T. *et al.* Interlayer interaction and electronic screening in multilayer graphene investigated with Angle-Resolved Photoemission Spectroscopy. *Phys. Rev. Lett.* **98**, 206802 (2007).
20. Latil, S. & Henrard, L. Charge carriers in few-layer graphene films. *Phys. Rev. Lett.* **97**, 036803 (2006).
21. Johansson, L. I., Xia, C. & Virojanadara, C. Na induced changes in the electronic band structure of graphene grown on C-face SiC. *Graphene* **2**, 1 (2013).
22. Avila, J. *et al.* ANTARES, a scanning photoemission microscopy beamline at SOLEIL. *JPCS* **425**, 192023 (2013).
23. Avila, J. *et al.* Exploring electronic structure of one-atom thick polycrystalline graphene films: A nano angle resolved photoemission study. *Sci. Rep.* **3**, 2349 (2013).
24. Kim, K. S. *et al.* Coexisting massive and massless Dirac fermions in symmetry-broken bilayer graphene. *Nature Mater.* **12**, 887–892 (2013).
25. Hohenberg, P. & Kohn, W. Inhomogeneous Electron Gas. *Phys. Rev.* **136**, B864 (1964).
26. Kohn, W. & Sham, L. J. Self-Consistent Equations Including Exchange and Correlation Effects. *Phys. Rev.* **140**, A1133 (1965).
27. Kresse, G. & Hafner, J. Ab initio molecular dynamics for liquid metals. *Phys. Rev. B* **47**, 558 (1993).
28. Kresse, G. & Furthmüller, J. Efficient iterative schemes for ab initio total-energy calculations using a plane-wave basis set. *Phys. Rev. B* **54**, 11169 (1996).
29. Blöchl, P. E. Projector augmented-wave method. *Phys. Rev. B* **50**, 17953 (1994).
30. Perdew, J. P., Burke, K. & Ernzerhof, M. Generalized gradient approximation made simple. *Phys. Rev. Lett.* **77**, 3865 (1996).

Acknowledgments

Author contributions

L.I.J. and C.V. conceived the experiments. L.I.J., C.X., C.V., J.A., S.L. and M.C.A. performed the experiments and the data analysis. R.A. and I.A.A. were responsible for the band structure calculations. L.I.J., C.V. and R.A. wrote the manuscript with input from all other co-authors.

Additional information

Supplementary information accompanies this paper at http://www.nature.com/scientificreports

Competing financial interests: The authors declare no competing financial interests.

How to cite this article: Johansson, L.I. *et al.* Multiple π-bands and Bernal stacking of multilayer graphene on C-face SiC, revealed by nano-Angle Resolved Photoemission. *Sci. Rep.* **4**, 4157; DOI:10.1038/srep04157 (2014).